Surface and Step Conductivities on Si(111) Surfaces

Sven Just,[1] Marcus Blab,[1] Stefan Korte,[1] Vasily Cherepanov,[1] Helmut Soltner,[2] and Bert Voigtländer[1,*]

[1]*Peter Grünberg Institut (PGI-3) and JARA-Fundamentals of Future Information Technology,*
Forschungszentrum Jülich, 52425 Jülich, Germany
[2]*Central Institute of Engineering, Electronics and Analytics (ZEA-1), Forschungszentrum Jülich, 52425 Jülich, Germany*
(Received 9 February 2015; published 3 August 2015)

Four-point measurements using a multitip scanning tunneling microscope are carried out in order to determine surface and step conductivities on Si(111) surfaces. In a first step, distance-dependent four-point measurements in the linear configuration are used in combination with an analytical three-layer model for charge transport to disentangle the 2D surface conductivity from nonsurface contributions. A termination of the Si(111) surface with either Bi or H results in the two limiting cases of a pure 2D or 3D conductance, respectively. In order to further disentangle the surface conductivity of the step-free surface from the contribution due to atomic steps, a square four-probe configuration is applied as a function of the rotation angle. In total, this combined approach leads to an atomic step conductivity of $\sigma_{\text{step}} = (29 \pm 9)\ \Omega^{-1}\,\text{m}^{-1}$ and to a step-free surface conductivity of $\sigma_{\text{surf}} = (9 \pm 2) \times 10^{-6}\ \Omega^{-1}/\square$ for the Si(111)-(7 × 7) surface.

The increasing importance of surface conductance compared to conductance through the bulk in modern nano-electronic devices calls for a reliable determination of the surface conductivity in order to minimize the influence of undesired leakage currents on the device performance or to use surfaces as functional units. A model system for corresponding investigations is the Si(111)-(7 × 7) surface. Over the years a wide range of values for the conductivity of this surface has been reported, spanning several orders of magnitude [1], and the latest measurements still deviate by a factor of 2 to 3 [2,3]. The main difficulty in measuring the surface conductivity is to separate the 2D conductance at the surface from the conductance through other channels, e.g., the bulk and the space charge layer.

Here, we use a four-tip scanning tunneling microscope (STM) [4] for distance-dependent measurements of the four-point resistance on Si(111), as shown in the inset in Fig. 1 for a linear tip arrangement, in combination with a three-layer model for charge transport. This method allows for the separation of the surface conductance from other contributions due to the characteristic probe spacing dependency of different conductance channels. Further on, we analyze the anisotropy of the surface conductance caused by the influence of atomic steps, which allows us to determine the conductivity of a single step and the step-free surface.

Analytic equations relating the measured four-point resistance to a conductivity can be obtained easily for pure 2D or 3D geometries, i.e., four tips positioned on a conducting sheet (surface) or on a half space (bulk), as [1]

$$R_{2D}^{4p} = \frac{\ln 2}{\pi \sigma_{2D}} \quad \text{and} \quad R_{3D}^{4p} = \frac{1}{2\pi \sigma_{3D}} s^{-1}, \qquad (1)$$

with an equidistant probe spacing s, the 2D surface conductivity σ_{2D}, and the 3D bulk conductivity σ_{3D}. The equation for the 2D case shows the hallmark of a 2D channel, namely, the fact that the surface conductance is independent of the probe spacing, while the conductance
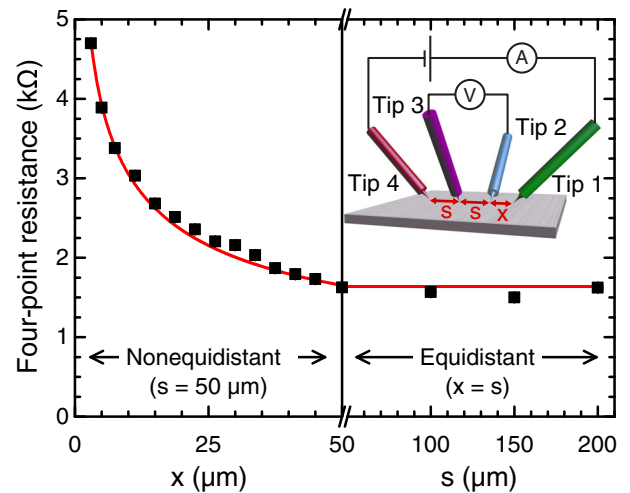

FIG. 1 (color online). Four-point resistance of a Bi-terminated Si(111)-($\sqrt{3} \times \sqrt{3}$)R30° sample as a function of the probe distances s and x for the equidistant (right half) and the nonequidistant configuration (left half). The red solid line represents the behavior expected for a pure 2D conductance with $\sigma_{Bi} = (1.4 \pm 0.1) \times 10^{-4}\ \Omega^{-1}/\square$. In the inset the linear measurement configuration is shown.

through a 3D channel depends on the distance s of the four probes. In order to minimize the number of tips to be repositioned, we preferentially use a nonequidistant spacing in which three tips remain at a mutual distance of $s = 50$ μm, while only the distance x between tip 1 and tip 2 is varied (Fig. 1). In this nonequidistant setup the hallmark of the constant four-probe resistance is lost for the 2D case since Eq. (1) has to be modified as it is shown in detail in Refs. [5–7] and as it is also summarized very briefly in the Supplemental Material [8].

The four-point resistance measured on a Si(111) − $(\sqrt{3} \times \sqrt{3})R30°$ Bi-terminated (1 monolayer) surface of an n-doped sample (2 kΩ cm) is shown in Fig. 1 for the nonequidistant configuration with distances $x \leq s = 50$ μm, and for the equidistant configuration with distances $x = s \geq 50$ μm (details about the sample preparation and measurement procedure are described in the Supplemental Material [8]). The constant behavior in the equidistant range $s \geq 50$ μm indicates a pure 2D character of conductance. Another indicator for 2D surface transport is the fact that the four-point resistance, which is expected considering only the bulk conductivity, is several orders of magnitude larger than the observed one. Therefore, we compare the experimental data to a 2D model, and a good correspondence is obtained for $\sigma_{Bi} = (1.4 \pm 0.1) \times 10^{-4}$ $\Omega^{-1}/\square$ (the solid red line), confirming that the charge transport in the Bi-terminated Si(111) sample occurs almost exclusively through the 2D surface channel. Similar results were found for two differently doped samples.

Subsequently, the distance dependence of the four-point resistance was measured on a clean Si(111)-(7 × 7) sample. The results for an n-doped sample (700 Ω cm) are shown in Fig. 2. The observed decreasing four-point resistance for increasing the equidistant probe spacing s indicates that a nonsurface channel contributes to the charge transport, since a pure 2D conduction exhibits a constant behavior in the equidistant region (cf. Fig. 1). Thus, the measured four-point resistance should be modeled by a conductance channel through the surface states as well as additional contributions from the bulk and a near-surface space charge layer. However, in this case Eq. (1) cannot be applied.

Often, an approximation of a parallel circuit consisting of the four-point resistance of the surface and the bulk (plus the space charge layer) is used [6], but this approach has two shortcomings. First, a complete separation of the surface conduction channel and the bulk is assumed. Second, the two-point resistances, not the four-point resistances, determine which amount of current flows through the surface layer and which part through the bulk or space charge layer. So, the preferred way for the current to split up depends on the details of the injection, e.g., the size of the current injecting contact (the tip diameter) [14]. Thus, if more than one current path exists, the four-point resistance depends on possible transitions between charge
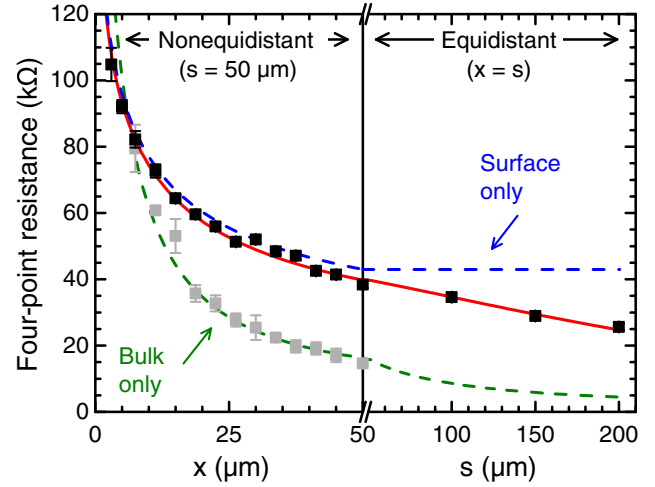

FIG. 2 (color online).   Four-point resistance of an n-doped Si(111)-(7 × 7) sample as a function of the probe distances s and x for the equidistant and the nonequidistant configuration. A three-layer model for charge transport yields the solid red line with $\sigma_{2D} = (5.1 \pm 0.7) \times 10^{-6}$ $\Omega^{-1}/\square$ located between the two limiting cases of a pure surface conductance (the dashed blue line) and a pure bulk conductance (the dashed green line). If the Si(111) surface is hydrogen terminated, the surface contribution vanishes completely and the remaining bulk conductance can directly be measured (gray data points).

transport channels as well as on the properties of the current injecting contacts, so that the well-known statement that the four-point resistance measured on the surface is independent of the contact resistances is not completely true.

In order to describe the charge transport through the different channels more accurately, we use an analytically derived three-layer model for conductance. In this model, the bulk enters with its known conductivity, while the surface conductivity is the parameter to be determined by a fit to the data. The space charge layer is approximated by an intermediate layer with a certain thickness and conductivity. These two values are obtained by the solution of the Poisson equation, which considers the known Fermi level pinning of the Si(111)-(7 × 7) surface [15,16]. Nevertheless, the use of the bulk doping concentration as an initial parameter in this calculation in order to determine the width and average conductivity of the space charge layer is not sufficient to describe the data in Fig. 2. However, it is known that high-temperature annealing up to 1200 °C performed for cleaning the Si(111) surface causes a dopant redistribution and an additional p-type doping in the near-surface region due to boron in-diffusion [17–20] or the possible formation of near-surface single vacancies [21]. These effects can lead to a reduced carrier concentration in the space charge layer. Generally, the details of the modification of the near-surface doping depend greatly on the specific method and setup used for sample preparation. We find that the experimental data can be described well for a conductivity of 2.5×10^{-4} Ω^{-1} m^{-1} and a

thickness of 3.1 μm for the intermediate layer representing the space charge layer. This quite approximate modeling of the space charge region as only one layer with constant conductivity seems to be sufficient, as the surface conductivity obtained from the fit to the measured data turns out to be insensitive to the specific properties of the intermediate layer.

Overall, the three-layer model results in a much more accurate description of the measured four-point resistance than the simple parallel-circuit model since it avoids the artificial separation between the surface and the nonsurface channels and takes into account the injection geometry giving rise to a charge transport inside and between the layers according to their properties. The analytical derivation of the model is described in detail in the Supplemental Material [8].

The best fit to the measured four-point resistance using the three-layer model is shown as a solid red line in Fig. 2 and results in a surface conductivity of $\sigma_{2D} = (5.1 \pm 0.7) \times 10^{-6} \, \Omega^{-1}/\square$. For comparison, the two limiting cases are marked in Fig. 2: The four-point resistance arising from a pure 2D conductivity σ_{2D} is shown as a dashed blue line, while the four-point resistance induced by a pure 3D conductance, with its $1/s$ behavior in the equidistant configuration, is indicated as a dashed green line featuring a bulk conductivity value, which is confirmed by the additional experiment described below. In the nonequidistant region the measured four-point resistance is close to the one expected from a pure surface conductance (less than 6% deviation for $x \leq 50$ μm), but for larger probe spacing an increasing deviation from the 2D behavior is observed. This reflects the well-known general tendency that the conductance is more surface dominated for small probe distances, while a nonsurface contribution develops more significantly for larger distances [1]. However, the observed four-point resistance does not approach the $1/s$ bulk behavior for $s \geq 50$ μm because the space charge layer blocks the charge transport into the bulk due to the low conductivity of the depletion zone. So, the four-point resistance in the equidistant range particularly reflects the properties of the space charge layer and the bulk, while the nonequidistant region is more suitable for the determination of the surface conductivity. In total, the three-layer model including the intermediate layer describes the experimentally observed behavior very well. Results obtained for other doping levels are shown in the Supplemental Material [8] and confirm the results presented above.

An additional experiment is used to explore whether the bulk conductivity can be measured directly with the four-probe setup after removing the surface conductance channel. A hydrogen termination of the Si(111) surface by a treatment in HF, resulting in the formation of the Si(111)-(1 × 1)-H, is known to remove the surface states present on the 7 × 7 surface [22]. The gray data points in Fig. 2 show the distance dependence of the four-point

resistance in the nonequidistant region measured on a hydrogen-terminated Si(111) sample. The dashed green line corresponds to a fit using a pure 3D bulk behavior with a resistivity of $\rho_{3D} = (580 \pm 70) \, \Omega$ cm, which is close to the macroscopically measured nominal bulk resistivity of $(700 \pm 50) \, \Omega$ cm and therefore confirms that, without surface states, a pure 3D bulk conductance is obtained.

While the distance-dependent four-point measurements could disentangle the surface conductivity from nonsurface contributions to charge transport, the influence of atomic steps located on the (7 × 7)-reconstructed Si surface has not been considered up to now. The conductivity arising from a single step for a current passing through it can be treated as scalar quantity. However, if a larger surface area is taken into account, the step array leads, on average, to an anisotropic conductivity described by the tensor components $\sigma^{\parallel}$ along the step edges and $\sigma^{\perp}$ perpendicular to the step edges [23]. So, the anisotropic conductance is a macroscopic (mean field) result of the different number of step edges per unit length along different current paths. It turns out that the linear four-point measurement configuration (Fig. 1) is not sensitive to a two-dimensional conductance anisotropy [24]. However, in a square arrangement of the four probes, as shown in Fig. 3(c), an angle-dependent four-point resistance is obtained from the solution of the Poisson equation for an anisotropic 2D sheet [24,25]

$$R(\theta) = C \ln\left(\frac{(\frac{\sigma^{\parallel}}{\sigma^{\perp}} + 1)^2 - 4\cos^2\theta\sin^2\theta(\frac{\sigma^{\parallel}}{\sigma^{\perp}} - 1)^2}{(\sin^2\theta + \frac{\sigma^{\parallel}}{\sigma^{\perp}}\cos^2\theta)^2}\right), \quad (2)$$

with $C = 1/(4\pi\sqrt{\sigma^{\parallel}\sigma^{\perp}})$.

Results for the measured anisotropic four-point resistance on an n-doped Si(111)-(7 × 7) sample (700 Ω cm) for a probe spacing of $s = 50$ μm are shown in Fig. 3(a) as a function of the rotation angle θ relative to the step direction. The four sets of differently colored data points in angle increments of 5° arise from the fact that for one fixed orientation of the probes four different rotation angles can be realized by successively assigning different probes as current and voltage probes.

A fit of Eq. (2) to the experimental data is shown as a dotted blue line in Fig. 3(a), describing the angle dependence quite well [26]. Nevertheless, the mean field approach applied so far assumes only straight step edges. However, the typical step structure present on our 0.25° misoriented Si(111)-(7 × 7) sample surface shown in Fig. 3(b) consists of steps aligned mainly along two directions with average angles of $\alpha \approx 8°$ and $\beta \approx 21°$ with respect to the average step orientation (indicated as red lines), which now defines $\sigma^{\parallel}$ and $\sigma^{\perp}$. This average step orientation arises from the macroscopic azimuthal direction of the sample miscut and is not aligned with the low-index orientations of the step edges. To model this more complicated nonparallel step pattern, we consider as a first-order approximation a
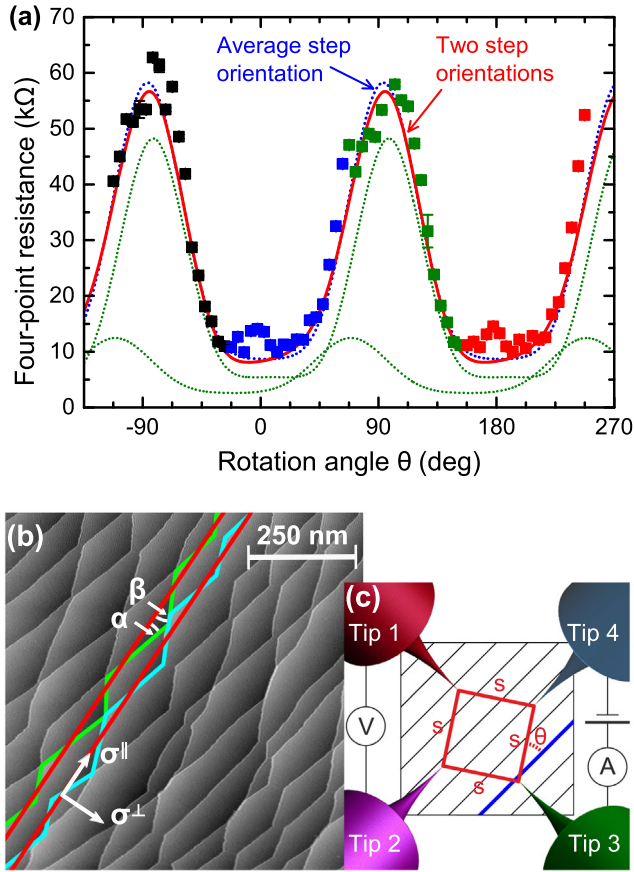
FIG. 3 (color online).   (a) Four-point resistance measured on a Si(111)-(7 × 7) surface in the square configuration [shown in (c)] with $s = 50\ \mu m$ as a function of rotation angle θ between the average step orientation and the line connecting the current injecting tips (the colored data points). The fits to the data using either only one average step direction or a superposition of two step orientations (the respective parts are shown as green dotted lines) are indicated as a dotted blue line and a solid red line, respectively. (b) STM image of the Si(111)-(7 × 7) surface showing the representative step arrangement on the sample. Two adjacent step edges are highlighted (the solid green and blue lines), consisting of two main step directions indicated by the angles α and β relative to the average step orientation (the solid red lines).

superposition of two step orientations with angles α and β relative to the average step orientation weighted with their respective portions extracted from Fig. 3(b). This leads to a slightly skewed curve shown as a solid red line in Fig. 3(a), which consists of an amount of 70% and 30% of the two single contributions, respectively (the dotted green lines). The model including the two step orientations describes the data as well as Eq. (2) but contains a better approximation of the sample step structure, and it results in $\sigma^{\parallel} = (9 \pm 2) \times 10^{-6}\ \Omega^{-1}/\square$ and $\sigma^{\perp} = (1.7 \pm 0.4) \times 10^{-6}\ \Omega^{-1}/\square$, with an anisotropy ratio of $\sigma^{\parallel}/\sigma^{\perp} \approx 5$. The geometric mean $\sqrt{\sigma^{\parallel}\sigma^{\perp}} = (3.9 \pm 0.6) \times 10^{-6}\ \Omega^{-1}/\square$ has nearly the same value within the error tolerances as the surface

conductivity σ_{2D} obtained in the linear configuration. Thus, the two independent methods, the distance-dependent linear configuration and the angle-dependent square configuration, yield the same results for the surface conductivity.

As a last step, we approximate the measured mean field anisotropic conductivity by the scalar resistivities of a step-free terrace ρ_{surf} and a single step ρ_{step}. Considering first the direction parallel to the steps, no step edges have to be crossed by the current, which results in the relation

$$1/\sigma^{\parallel} = \rho^{\parallel} = \rho_{surf}. \tag{3}$$

Second, the resistivity perpendicular to the step edges is composed of additive contributions from the steps and the step-free terraces and can be expressed as series resistance, resulting in [23]

$$1/\sigma^{\perp} = \rho^{\perp} = \rho_{surf} + \rho_{step}/d_{step}^{\perp}, \tag{4}$$

with $d_{step}^{\perp}$ denoting the average distance between the steps. From the two relations in Eqs. (3) and (4), the conductivity of the step-free Si(111)-(7 × 7) surface can finally be disentangled from the influence of the step conductivity as $\sigma_{surf} = (9 \pm 2) \times 10^{-6}\ \Omega^{-1}/\square$, and $\sigma_{step} = (29 \pm 9)\ \Omega^{-1}m^{-1}$. The value of the surface conductivity σ_{surf} is a factor of 2 to 6 larger than the values obtained in recent experiments [2,3]. Such smaller values may be explainable, as these experiments are based on a more indirect comparison of the conductivity before and after quenching the surface states by adsorption of atoms or molecules. For the quenched system several conditions have to be fulfilled: (a) the surface states of the surface under study are completely quenched, (b) the space charge layer conductivity is not influenced by the adsorbed layer, and (c) the adsorbed layer induces no (additional) surface conductance. If one of these conditions is not fulfilled, these experiments based on the difference method result in different values for the surface conductivity.

From a comparison of the surface resistivity and the step resistivity, the following relation is obtained. The resistance of one step (per unit length) corresponds to the resistance of a segment of the step-free Si(111)-(7 × 7) surface (per unit length) of a width of 300 nm. For our sample with a step density of 14 steps/μm, the contribution of the step resistance to the total resistance has a substantial amount of 80% for a current flowing in the perpendicular direction. In general, the presence of steps will reduce the surface conductivity of the Si(111)-(7 × 7) considerably— however, in a very predictable manner.

In conclusion, we combined the distance-dependent linear configuration for four-point resistance measurements on Si(111) surfaces with a three-layer model for charge transport in order to disentangle the surface conductivity from nonsurface contributions (bulk and space charge layer

conductivity). The influence of atomic surface steps is obtained by measurements in the angle-dependent square configuration resulting in a step-free surface resistivity of $\rho_{surf} = (116 \pm 26)$ k$\Omega/\square$ and a step resistivity of $\rho_{step} = (3.4 \pm 1) \times 10^{-2}$ Ωm for the Si(111)-(7 × 7) surface. These two generic methods can easily be used to determine surface conductivities of other mixed 2D-3D systems, like different semiconductors or topological insulators.

---

*Corresponding author.
b.voigtlaender@fz-juelich.de

[1] P. Hofmann and J. W. Wells, J. Phys. Condens. Matter **21**, 013003 (2009).
[2] M. D'angelo, K. Takase, N. Miyata, T. Hirahara, S. Hasegawa, A. Nishide, M. Ogawa, and I. Matsuda, Phys. Rev. B **79**, 035318 (2009).
[3] B. V. C. Martins, M. Smeu, L. Livadaru, H. Guo, and R. A. Wolkow, Phys. Rev. Lett. **112**, 246802 (2014).
[4] V. Cherepanov, E. Zubkov, H. Junker, S. Korte, M. Blab, P. Coenen, and B. Voigtländer, Rev. Sci. Instrum. **83**, 033707 (2012).
[5] J. W. Wells, J. F. Kallehauge, and P. Hofmann, Surf. Sci. **602**, 1742 (2008).
[6] J. W. Wells, K. Handrup, J. F. Kallehauge, L. Gammelgaard, P. Boggild, M. B. Balslev, J. E. Hansen, P. R. E. Petersen, and P. Hofmann, J. Appl. Phys. **104**, 053717 (2008).
[7] M. Wojtaszek, J. Lis, R. Zuzak, B. Such, and M. Szymonski, Appl. Phys. Lett. **105**, 042111 (2014).
[8] See Supplemental Material at http://link.aps.org/supplemental/10.1103/PhysRevLett.115.066801, which includes Refs. [9–13], for details on the sample preparation and measurement procedure, additional experimental results for different doping levels, and a description of the three-layer conductance model.
[9] K. Romanyuk, J. Myslivecek, V. Cherepanov, T. Sekiguchi, S. Yoshida, K. M. Itoh, and B. Voigtländer, Phys. Rev. B **75**, 241309 (2007).
[10] T. Uetake, T. Hirahara, Y. Ueda, N. Nagamura, R. Hobara, and S. Hasegawa, Phys. Rev. B **86**, 035325 (2012).
[11] C. Blömers, T. Grap, M. I. Lepsa, J. Moers, S. Trellenkamp, D. Grützmacher, H. Lüth, and T. Schäpers, Appl. Phys. Lett. **101**, 152106 (2012).
[12] C. Durand, M. Berthe, Y. Makoudi, J. Nys, R. Leturcq, P. Caroff, and B. Grandidier, Nanotechnology **24**, 275706 (2013).
[13] J. D. Jackson, Classical Electrodynamics, 3rd ed. (Wiley, New York, 1999).
[14] C. M. Polley, W. R. Clarke, J. A. Miwa, M. Y. Simmons, and J. W. Wells, Appl. Phys. Lett. **101**, 262105 (2012).
[15] H. Lüth, Solid Surfaces, Interfaces and Thin Films (Springer-Verlag, Berlin, 2001).
[16] G. Hollinger and F. J. Himpsel, J. Vac. Sci. Technol. A **1**, 640 (1983).
[17] M. Liehr, M. Renier, R. A. Wachnik, and G. S. Scilla, J. Appl. Phys. **61**, 4619 (1987).
[18] S. S. Iyer, S. L. Delage, and G. J. Scilla, Appl. Phys. Lett. **52**, 486 (1988).
[19] H. M. Zhang, K. Sakamoto, G. V. Hansson, and R. I. G. Uhrberg, Phys. Rev. B **78**, 035318 (2008).
[20] D. J. Robbins, A. J. Pidduck, J. L. Glasper, I. M. Young, and C. Pickering, Thin Solid Films **183**, 299 (1989).
[21] S. Bensalah, J.-P. Lacharme, and C. A. Sébenne, Phys. Rev. B **43**, 14441 (1991).
[22] S. Bouzidi, F. Coletti, J. M. Debever, P. A. Thiry, P. Dumas, and Y. J. Chabal, Phys. Rev. B **45**, 1187 (1992).
[23] I. Matsuda, M. Ueno, T. Hirahara, R. Hobara, H. Morikawa, C. Liu, and S. Hasegawa, Phys. Rev. Lett. **93**, 236801 (2004).
[24] T. Kanagawa, R. Hobara, I. Matsuda, T. Tanikawa, A. Natori, and S. Hasegawa, Phys. Rev. Lett. **91**, 036805 (2003).
[25] V. M. Tatarnikov, Meas. Tech. **13**, 877 (1970).
[26] Since Eq. (2) considers a 2D conductivity exclusively, a correction factor for the 6% nonsurface contribution to charge transport determined by the linear probe measurements has been taken into account.